8-2020

Hodographic Analysis of Na Lidar Data to Measure Atmospheric Gravity Wave Parameters

Jeffrey Ormsby
Utah State University

Hodographic Analysis of Na Lidar Data to Measure Atmospheric Gravity Wave Parameters

Jeffrey Ormsby

Titus Yuan

PHYS 4900 Research in Physics

Department of Physics, Utah State University, Logan, UT

The Utah State University Sodium lidar observatory, hosted in Science and Engineering Research building at Logan campus, measures the winds and temperature near the boundary of eddy diffusion dominated upper atmosphere between 80 and 110-km, where various atmospheric internal waves, especially atmospheric gravity waves (buoyancy waves), play important roles in the dynamics and chemistry. In this study, using a hodographic algorithm, the lidar data were analyzed to extract critical parameters of these gravity waves detected in this region, such as horizontal propagating phase velocity and wavelength. Results were compared with the independent Advanced Atmospheric Temperature Mapper (AMTM) observations, co-located at Utah State University.

Introduction

Atmospheric gravity waves are ubiquitous and are a key aspect of space weather due to their role in various ion-neutral coupling processes. They play an important role in energy transfer between atmospheric layers as their momentum changes when they propagate vertically and horizontally, while their amplitudes can grow exponentially going into the upper atmosphere due to decreasing atmospheric density.

Through hodographic analysis techniques, important parameters of these gravity waves, such as horizontal wavelength and phase velocity, can be identified from a single point measurements of temperature and horizontal wind perturbations (though, obviously, many data points must be used to ensure accuracy of the results). This appealing method therefore allows the derivations of GW horizontal parameters to be calculated through single point observations, for example those by lidar. However, the accuracy of this method has been a controversial topic within the physics community (Zhang, et al., 2004).

By identifying GW parameters using Na lidar data and verifying these results with the co-located USU Advanced Mesospheric Temperature Mapper (AMTM) observations, which is capable of horizontal GW observation, the accuracy of this method can be either corroborated or disputed. Corroboration of this method could lead to its wider acceptance and a greater ability to research and understand atmospheric gravity waves.

Procedure

Sodium lidar data for nightly temperature, zonal (east-west), and meridional (north-south) wind are stored in separate files which contain observations for temperature and wind speed values (including uncertainties) at various altitudes over a series of time intervals. These data were read in and the data from each file was stored in a 2D array. Next, values in the arrays were compared to their errors and data values which had an error in excess of 5% were removed.

Line-of-sight wind data was converted to horizontal wind using

$$v_{N,E} = v_{LOS} \cos\theta \quad (1)$$

where v_N is the magnitude of the north wind and v_E is the magnitude of the east wind and the angles of the north and east beams were 30° and 20° respectively. This correction was applied to wind speed readings as well as error readings. These zonal and meridional wind readings were then used to find the horizontal wind's magnitude and direction using the following equations, respectively:

$$v_{horiz} = \sqrt{v_N^2 + v_E^2} \tag{2}$$

$$\theta_{horiz} = atan\left(\frac{v_E}{v_N}\right) \tag{3}$$

To remove slow varying background value and, thus, calculate the perturbations, a third-order polynomial fit was applied to the remaining data. This fit was then subtracted from the raw data at each point to isolate the gravity wave induced temperature and wind perturbations. The data were then linearly interpolated and new data sets of values ranging from 85-km to 100-km at 1-km intervals were constructed.

With the continuous reconstructed data, an FFT was applied to each data set. The FFTs identified strong modulations at periods of 12 and 3 hours in the temperature data and 12, 6, and 3 hours in the wind data. Initially, the data sets were fitted using the equation

$$F(t) = Asin(\omega t) + Bcos(\omega t) \tag{4}$$

with ω equal to 2π/12 with the goal of isolation the 12-hour tidal wave modulation, which is a regular large global scale wave generated by the atmosphere absorption of solar radiation. This fit was subtracted from the data sets and the modified data sets were then fitted to the same equation with ω equal to 2π/3 to remove the 3-hour modulation. This fit was then used to reconstruct ideal data sets and identify the gravity wave parameters.

When this approach did not produce good fitting and the questionable perturbation results, a new fitting function was created which incorporated both of the previous functions at the same time (with ω equal to 2π/12):

$$F(t) = A\sin(\omega t) + B\cos(\omega t) + C\sin(4\omega t) + D\cos(4\omega t)$$

(5)

However, it is found that this approach does not generate an ideal fit either and, thus, affects the key perturbation calculation. A closer inspection of the FFT graphs revealed the 6-hour strong periodic modulation in the wind data that was not present in the temperature data. A final fitting function was constructed which incorporated all three strong wave modulations

$$F(t) = A\sin(\omega t) + B\cos(\omega t) + C\sin(2\omega t) + D\cos(2\omega t) + E\sin(4\omega t) + F\cos(4\omega t)$$

(6)

with ω equal to 2π/12, allowing all three strong modulations identified by the FFT to be fitted simultaneously. Next, rather than removing background data from the data sets, ideal data sets were constructed using the equation

$$F(t) = E\sin(\omega t) + F\cos(\omega t)$$

(7)

with ω equal to 2π/12 and E and F equal to the values identified for E and F in the least squares fitting of (6).

The E and F coefficients for each altitude of each data set were stored in Excel and used to visually identify vertical wavelength. Next, the phase difference for each pair of north and east wind data points was calculated using

$$\Phi_{diff} = atan\left(\frac{E_E}{F_E}\right) - atan\left(\frac{E_N}{F_N}\right)$$

(8)

where E and F once again correspond to the coefficients identified by the least squares fitting in (6). Once the zonal and meridional wind perturbations are calculated, along with their phase difference, a series of equations from the paper *Advanced hodograph-based analysis technique to derive gravity wave parameters from Lidar observations* (Strelnikova, et al., 2019) was used to identify the gravity wave parameters. These equations are [with the exception of (13) and (15)] as follows:

$$\Phi_{uv} = \hat{u} \cdot \hat{v} \cdot cos(\varphi_u - \varphi_v).$$

(9)

which is used to identify the wave propagation direction in (10), where $\hat{u} \wedge \hat{v}$ are the calculated zonal and meridional wind perturbations and $\varphi_u - \varphi_v$ is the phase difference between the two orthogonal wind components in (8).

$$\xi = \frac{1}{2}(\pi n + \arctan(\frac{2\Phi_{uv}}{\widehat{v}^2 - \widehat{u}^2}))$$

(10)

which identifies the wave propagation direction,

$$2\widehat{u_{\parallel}}^2 = \widehat{u}^2 + \widehat{v}^2 + \sqrt{(\widehat{u}^2 - \widehat{v}^2)^2 + 4\Phi_{uv}^2}$$

(11)

and

$$2\widehat{u_{\perp}}^2 = \widehat{u}^2 + \widehat{v}^2 - \sqrt{(\widehat{u}^2 - \widehat{v}^2)^2 + 4\Phi_{uv}^2}$$

(12)

which identify wave amplitudes in ellipse coordinates,

$$f = 2\pi sin\varphi = 16.5/h$$

(13)

where f is the Coriolis frequency and φ is a function of latitude,

$$|\widehat{u_{\parallel}}|/|\widehat{u_{\perp}}| = \widehat{\omega}/f$$

(14)

where $\widehat{\omega}$ is the intrinsic frequency of the wave modulation,

$$N^2 = \frac{g}{T}(\frac{dT}{dz} + \frac{g}{C_p})$$

(15)

where N is the buoyancy frequency and T is temperature measured by the lidar, g is gravitational acceleration in mesopause region, C_p is specific heat,

$$k_{\parallel}^2 = m^2 \left(\frac{\widehat{\omega}^2 - f^2}{N^2 - \widehat{\omega}^2} \right)$$

(16)

where $k_{\parallel}$ is the GW's wave number and m is the wave number of the vertical wave propagation,

$$c_{\parallel} = \widehat{\omega}/k_{\parallel} \tag{17}$$

where $c_{\parallel}$ is the horizonal phase speed, and

$$c_z = \widehat{\omega}/m \tag{18}$$

where c_z is the vertical phase speed.

Results

Graphs were automatically generated for temperature, north wind, and east wind perturbations, FFTs (before and after applying each fitting function) at each altitude, as well as polar graphs of wind speeds displaying both raw data and idealized fitted data. For the purpose of brevity, not all 216 of these graphs can be displayed here. I will instead show examples of temperatures at 90 km and meridional wind at 95 km.

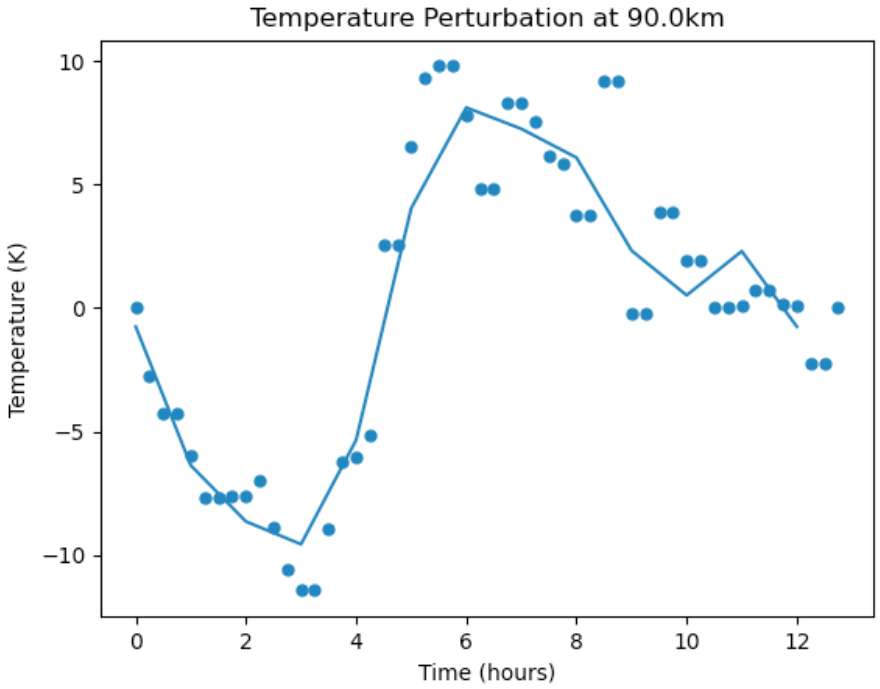

Fig. 1. Temperature perturbation raw data (points) with fitting function applied (solid line)

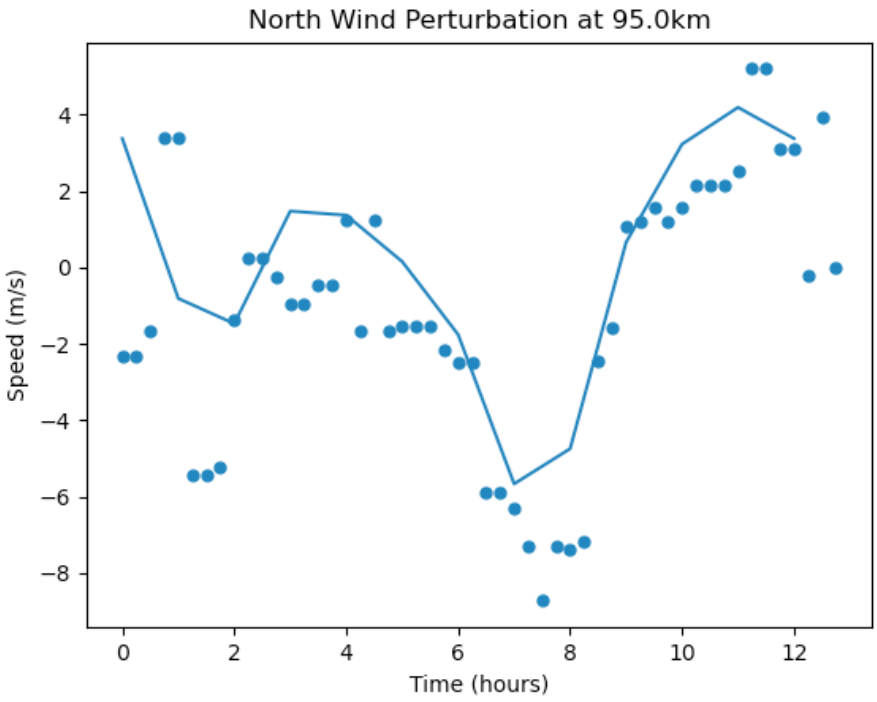

Fig. 2. North wind perturbation raw data (points) with fitting function applied (solid line)

In Fig. 1 and Fig. 2, the perturbation of temperature and north wind speed at 95 km can be seen. While there are a small number of outliers, the data for this region is fairly clean and the fit clearly matches the raw data.

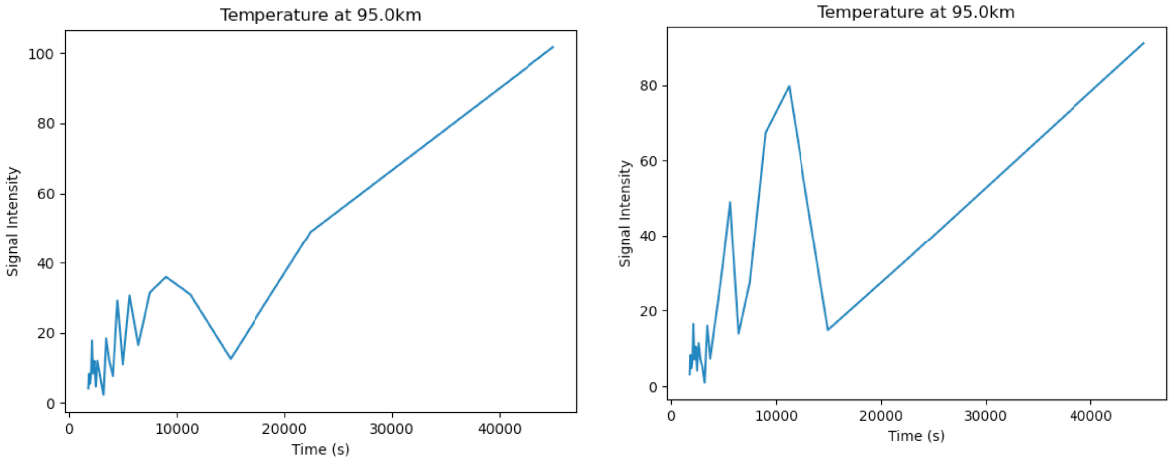

Fig. 3. Temperature FFT at 95 km before (left) and after (right) applying the final fitting function

In Fig. 3, we see the FFT results of temperature at 95 km which reveals the strong wave modulations at 12 and 3 hours.

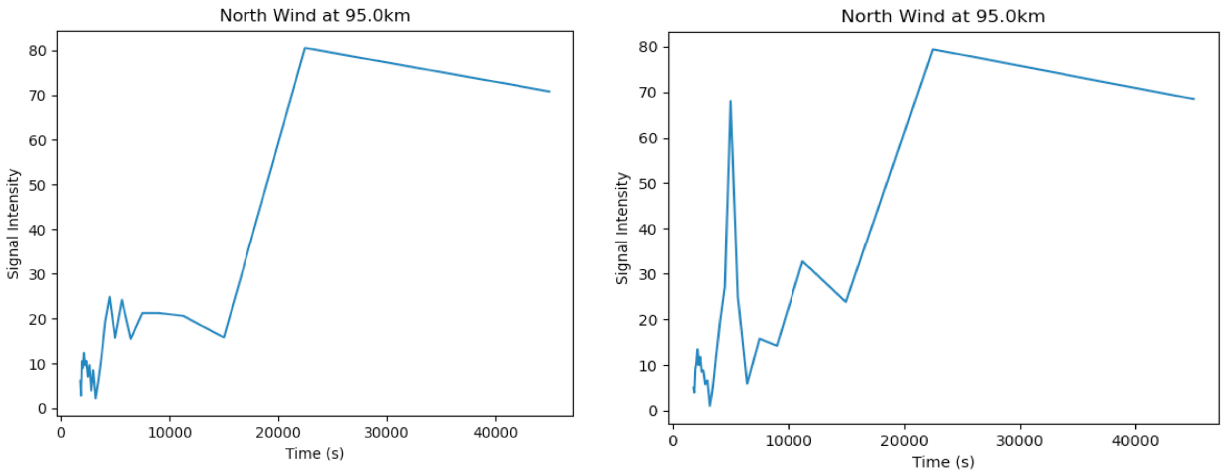

Fig. 4. North wind FFT at 95 km before (left) and after (right) applying the final fitting function

In Fig. 4, strong wave modulations in wind speed can be seen at 12, 6, and 3 hours. The FFTs for the east wind identified the same modulations.

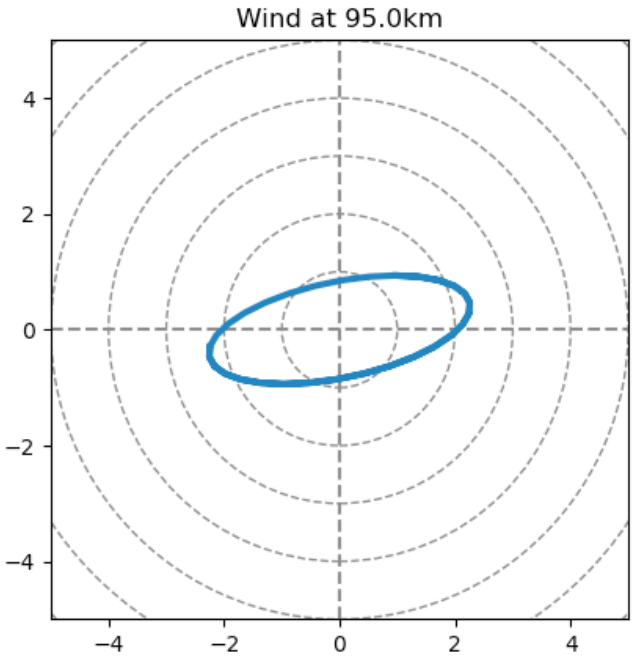

Fig. 5. Wind speed at 95 km

In Fig. 5, fitted wind speed at 95 km is plotted.

For each fitting function, the same value for $\frac{dT}{dz}$ and vertical wavenumber, m, was used.

These were $\frac{dT}{dz} = 0.965\,K/m$ and $m = \frac{1}{7.0}\,km$.

The results of the analysis using the fitting function (4) are as follows:

ξ	70.02	° E of N
$u_{\parallel}$	6.947	km/h
$u_{\perp}$	1.265	km/h
N	22.21	/h
$k_{\parallel}$	0.004367	/km
$\hat{\omega}$	1.582	/h
$\lambda_{\parallel}$	229.0	km
$c_{\parallel}$	362.3	km/h
c_z	11.08	km/h

Table 1. Results of analysis with one-function fitting

Likewise, the results of the analysis using the function (5) are as follows:

ξ	71.44	° E of N
$u_{\parallel}$	7.019	km/h
$u_{\perp}$	1.329	km/h
N	5.970	/h
$k_{\parallel}$	0.002525	/km
$\hat{\omega}$	1.040	/h
$\lambda_{\parallel}$	396.0	km
$c_{\parallel}$	412.0	km/h
c_z	7.283	km/h

Table 2. Results of analysis with two-function fitting

And finally, the results of the analysis using the three-function fitting (6) are as follows:

ξ	69.22	° E of N
$u_{\parallel}$	1.530	km/h
$u_{\perp}$	0.4549	km/h
N	65.26	/h
$k_{\parallel}$	0.01151	/km
$\hat{\omega}$	1.864	/h
$\lambda_{\parallel}$	86.89	km
$c_{\parallel}$	162.0	km/h
c_z	13.05	km/h

Table 3. Results of analysis with three-function fitting

Conclusion

The wildly varying results for each set of analysis demonstrates the importance of accurately fitting the data and the resulting wind perturbations. Even a small error can cause drastic discrepancies in the final results. While both the horizontal and vertical wavelengths seemed too high in Table 1, they became far more unreasonable in Table 2. Likewise, the intrinsic frequency in Table 1 did not match the observed frequency and it strayed even further in Table 2. While the more careful analysis done in Table 3 produced better results, it is difficult to say definitively how accurate these are. While they are reasonable, they could also be subject to unforeseen errors that would be revealed through further, even more complete analysis.

Appendix

Source code is available at https://github.com/jaormsby/Hodographs